Acta Mechanica Sinica (2021) 37(2):349–365
https://doi.org/10.1007/s10409-020-01002-w

RESEARCH PAPER

Quantitative characterization of damage-aggravation effect caused by progressive damage

Qindong Lin[1,2] · Shihai Li[1,2] · Chun Feng[1] · Dong Zhou[1]

Received: 7 April 2020 / Revised: 3 August 2020 / Accepted: 27 August 2020 / Published online: 4 January 2021

Abstract
Aiming at the progressive damage phenomenon in geotechnical field, it attempts to study the effect of progressive damage on the macro-bearing capacity. Firstly, based on the theoretical analysis of a two-dimensional plane inside representative volume element, it is proposed that progressive damage will occur if the bearing capacity of microplanes is different. Besides, "damage-aggravation effect" is proposed according to the difference between the macro-bearing capacity of entire plane and the sum of bearing capacity of all microplanes when progressive damage occurs. Secondly, progressive damage ratio K_t is proposed to quantify "damage-aggravation effect". Finally, based on the rod model, the correspondence between K_t and some influence factors is studied by theoretical analysis and numerical simulation. The results show that "damage-aggravation effect" does exist, and the macro-bearing capacity of entire plane is less than the sum of bearing capacity of all microplanes when progressive damage occurs. If the bearing capacity of rods in the rod model obeys uniform distribution, as the minimum of bearing capacity increases linearly, the macro-bearing capacity increases linearly, and K_t decreases inversely.

Keywords Progressive damage · Bearing strength · Damage-aggravation effect · Progressive damage ratio

1 Introduction

Progressive damage refers to micro-damage gradually occurs in different regions inside the research object under external load, and ultimately the entire object is destroyed. Progressive damage is widespread in the fields of composite material, industry, architecture and geotechnical engineering, and it has an important influence on the overall stability of structure. In the field of composite material, researchers studied the progressive damage process of new composite material (e.g. carbon fiber reinforced aluminum laminates) based on numerical simulation and experiment, and then proposed some corresponding progressive damage model to describe the progressive damage process [1–5]. In the industrial field, researchers conducted experiment and numerical simulation on typical components (e.g. wind turbine blade), and then proposed some damage model according to the damage characteristics of different components, which is helpful to accurately analyze their progressive damage process and durability [6–10]. In the field of architecture, many researchers analyzed the whole progressive damage process of architecture under different external load through numerical simulation, and discussed the effect of some influencing factors on the structural response [11–14].

In the geotechnical field, due to the complexity of geological structure and rock mechanical properties, there is an obvious progressive damage process. Some scholars studied the failure process of slope based on experiment and numerical simulation. The results show that the failure of slope is progressive, and the damage mainly occurs at the bottom of slope at the beginning. With the increase of time, more and more damage appears, and ultimately the entire slope collapses. Because of progressive damage, the stability of entire slope gradually decreases [15–20].

As a natural material, rock is formed by different mineral particles and cement materials under the long geological processes, and it has certain characteristics in terms of composition materials and microstructure. The microstructure of rock is often observed by micro-computed tomography

✉ Chun Feng
fengchun@imech.ac.cn

[1] Key Laboratory for Mechanics in Fluid Solid Coupling Systems, Institute of Mechanics, Chinese Academy of Sciences, Beijing 100190, China

[2] School of Engineering Science, University of Chinese Academy of Sciences, Beijing 100049, China

(CT), backscattered scanning electron microscope (BSE-SEM), energy dispersive spectroscopy (EDS), etc., and the observation results clearly show the complexity of rock microstructure [21, 22]. The pore is an important factor causing the complexity of rock microstructure, based on the low field nuclear magnetic resonance equipment and X-ray microcomputed tomography, the distribution characteristic of pore was investigated [23]. Besides, a continuous pore-size distribution is used to quantify the microstructure based on the small-angle neutron scattering (SANS) and backscatter SEM imaging [24]. The composition materials of rock are also complex, energy-dispersive spectrometry, optical petrographic microscope and back-scattered electron imaging are often used to accurately investigate the mineral composition of rock [25]. At the same time, laboratory experiment and numerical simulation are combined to study the heterogeneity of rock [26, 27].

These research results show that rock has the characteristics of compositional diversity, microstructure complexity, and local defect, which are closely related to the progressive damage process. Numerical simulation and laboratory experiment are important methods to study the progressive damage process under different external load. Based on the results of numerical simulation and experiment, the corresponding rupture nucleation processes and influencing factors are proposed [28–30]. In laboratory experiment, because the damage occurs mostly inside the rock, it is difficult to observe and count. Based on the advantages of non-destructive monitoring, dynamic real-time monitoring and easy calibration of the damage position, acoustic emission (AE) is often used to obtain the rock damage information in laboratory experiment. Based on the monitoring information of acoustic emission, it can be observed that the damage of rock specimen has obvious progressive features [31–34]. Besides, the research results show that progressive damage leads to the complex mechanical properties of rock, and the inflection points of strain–stress curve are closely related to the area and spatial distribution of crack [35–39]. Many scholars have established several constitutive models of rock based on statistical damage theory and other theories [40–45].

The causes of progressive damage process can be attributed to local defect, non-uniformity of geometry, non-uniformity of external load and non-uniformity of mechanical parameters. The change of these factors can affect the progressive damage process of model under external load and lead to the change of macro-bearing strength. For the local defect, studies have shown that as the size and number of defect increase, the bearing strength of model decreases [46, 47]. For the non-uniformity of geometry, Liu et al. [48] proposed an indicator H_{new} to quantify the geometric non-uniformity of the internal particles of rock, and the numerical results showed that the peak intensity decreases approximately linearly with the increase of H_{new}. For the non-uniformity of mechanical parameters, based on numerical simulation, it is found that the bearing strength of model decreases with the increase of the non-uniformity of mechanical parameters or the proportion of weaker materials [49, 50].

The progressive characteristics of damage have an important influence on the constitutive law and macro-bearing strength of rock. With regard to the progressive damage process, the current research focuses on: (1) the relationship between stress–strain curve and related damage stage (e.g. number, area, and position of crack planes); (2) proposing a new constitutive model to describe the complex mechanical characteristics of rock; (3) studying the changing law of macro-bearing strength when the mechanical parameters and geometrical parameters of rock change. However, in current research, the quantitative correspondence between the sum of bearing capacity of all crack planes inside the model and the macro-bearing capacity of model has not been studied.

Based on the bearing capacity of crack planes inside the research object, this paper attempts to establish a dimensionless indicator to achieve the quantitative study on the correspondence between the sum of bearing capacity of all crack planes and the macro-bearing capacity, and investigate the correspondence between the dimensionless indicator and some influencing factors. In "Methodology" section, the theoretical analysis of a two-dimensional plane inside the representative volume element is conducted. It is proposed that progressive damage will produce "damage-aggravation effect" compared to the simultaneous damage of all microplanes, then the dimensionless progressive damage ratio K_t is proposed. In "Parameter study" section, the correspondence between some influencing factors and K_t is analyzed theoretically based on the rod model, and the correspondence between the non-uniformity of bearing capacity and K_t is verified by numerical simulation.

2 Methodology

A two-dimensional plane inside the representative volume element is taken as the research object. Firstly, by analyzing the correspondence between the macro-bearing capacity F_{ma} of entire plane and the sum F_{sum} of bearing capacity of all microplanes in both cases of simultaneous damage and progressive damage, it is proposed that progressive damage will produce "damage-aggravation effect", and it is closely related to the non-uniformity of bearing capacity of microplanes. Then progressive damage ratio K_t, a dimensionless indicator, is proposed to quantify "damage-aggravation effect".

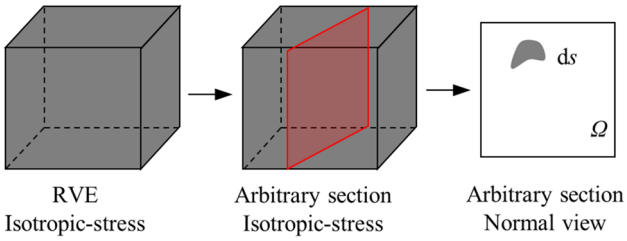

Fig. 1 Representative volume element

2.1 Difference of the macro-bearing capacity

The representative volume element (RVE) is a model for characterizing the mechanical properties of materials in mechanical analysis. A two-dimensional plane inside the RVE is shown in Fig. 1.

Before theoretically analyzing the macro-bearing capacity F_{ma}, two basic assumptions are proposed.

Assumption 1: The stress is same at any position inside the RVE. Since the RVE has the characteristic of "infinitesimal at the macro-scale", it can be assumed that the stress is same at any position inside the RVE to facilitate theoretical analysis. It means that the stress value of all microplanes is equal.

Assumption 2: The breaking criterions followed by all microplanes are the maximum tensile stress criterion and the Mohr–Coulomb criterion. Therefore, whether a microplane is broken or not can be judged by stress. If no damage occurs, the microplane still maintains elastic constitutive model and bears load, once the microplane breaks, it no longer bears load.

For the two-dimensional plane inside the RVE, it includes lots of microplanes, and every microplane can bear external force. The sum F_{sum} of bearing capacity of all microplanes is obtained by accumulating the bearing capacity of each microplane, it means that the external force on each microplane is equal to the bearing capacity of the microplane, and it can be concluded that F_{sum} denotes the force value that all microplanes can bear together.

2.1.1 Simultaneous damage

When all microplanes of the 2D plane break simultaneously, from the basic assumption 2, it can be known that all microplanes simultaneously satisfy the maximum tensile stress criterion (if tensile failure) or the Mohr–Coulomb criterion (if shear failure), so the stress value of microplanes is equal to the bearing strength. The basic assumption 1 indicates that the stress value of all microplanes is same before the damage of microplanes occurs. Therefore, it can be concluded that the bearing strength of all microplanes is same, and the macro-bearing capacity F_{ma} of entire plane is equal to the sum F_{sum} of bearing capacity of all microplanes. The expression of F_{sum} is written as

$$F_{sum} = \begin{cases} \iint_{\Omega} \sigma_t \mathrm{d}s, & \text{if tensile faliure,} \\ \iint_{\Omega} \sigma_s \mathrm{d}s, & \text{if shear faliure,} \end{cases} \tag{1}$$

where Ω denotes the integral domain (i.e., the area of entire plane) and s is integral variable, σ_t denotes the tensile strength of microplane, and σ_s denotes the shear strength of microplane.

The concept that the macro-bearing capacity F_{ma} of entire plane is equal to the sum F_{sum} of bearing capacity of all microplanes widely exists in the field of geotechnical engineering. For example, in the limit equilibrium method for calculating slope safety factor, it is considered that the anti-sliding force of entire slope is equal to the sum of anti-sliding force of all sliding slices. However, the above analysis shows that the precondition for $F_{ma} = F_{sum}$ is that all microplanes are destroyed simultaneously. Once the damage of microplanes occurs at different time, that is, the damage of all microplanes is progressive, the correspondence between F_{ma} and F_{sum} needs to be re-determined.

2.1.2 Progressive damage

Progressive damage means that the damage of all microplanes does not occur simultaneously. The strain strength distribution model, proposed by Li and Zhou [51], realizes the progressive damage process of entire plane. In this model, it is assumed that the strain strength of all microplanes is different, and the results show that progressive damage will lead to complex nonlinear mechanical properties.

It is known that the key to the appearance of progressive damage is the difference in bearing strength of microplanes. Therefore, by randomizing the bearing strength of microplanes, the correspondence between F_{ma} and F_{sum} is studied. Currently, uniform distribution function, weibull distribution function and normal distribution function are often used to randomize the mechanical parameters. Under the premise that the bearing strength obeys uniform distribution, the correspondence between F_{ma} and F_{sum} is studied when the plane bears uniaxial tensile load.

The progressive damage process of plane is plotted in Fig. 2. At the initial time of loading, the stress inside the RVE is low, no microplane meets the breaking criterion and no damage occurs. With the increase of stress, the microplanes with low tensile strength meet the breaking criterion firstly and these microplanes break. With the continuous increase of stress, more and more microplanes break, and ulti-

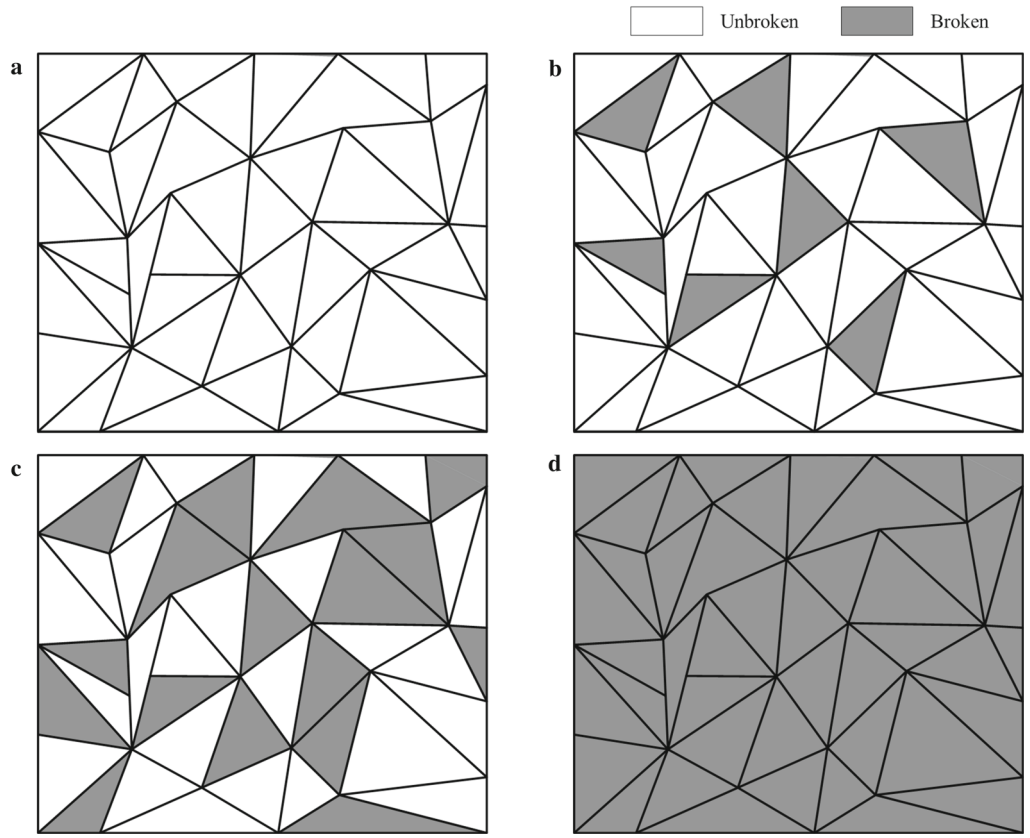

Fig. 2 Progressive damage process of plane. **a** No broken microplanes, **b** some broken microplanes, **c** more broken microplanes, and **d** all broken microplanes

mately the entire plane is broken. It can be observed that the microplanes of entire plane are divided into two categories: broken and unbroken. The unbroken microplanes still maintain the elastic constitutive model and bear load, while the broken microplanes no longer bear load. Therefore, it can be concluded that external force is only borne by unbroken microplanes.

Before investigating the correspondence between F_{ma} and F_{sum}, several key quantities are defined. S denotes the area of entire plane. Crack area S_{c} denotes the area of broken microplanes, and intact area S_{I} denotes the area of unbroken microplanes. Crack ratio α_{c} denotes the ratio of crack area S_{c} to the area of entire plane, and intact ratio α_{I} denotes the ratio of intact area S_{I} to the area of entire plane. In the process of tensile damage, these quantities can be written as

$$\alpha_{\mathrm{c}} = \begin{cases} 0, & \sigma < \sigma_{\min}, \\ \dfrac{\int_{\sigma_{\min}}^{\sigma} f(\xi)\mathrm{d}\xi}{\int_{\sigma_{\min}}^{\sigma_{\max}} f(\xi)\mathrm{d}\xi}, & \sigma_{\min} \le \sigma \le \sigma_{\max}, \\ 1, & \sigma_{\max} < \sigma, \end{cases} \tag{2}$$

$$\alpha_{\mathrm{I}} = \begin{cases} 1, & \sigma < \sigma_{\min}, \\ \dfrac{\int_{\sigma}^{\sigma_{\max}} f(\xi)\mathrm{d}\xi}{\int_{\sigma_{\min}}^{\sigma_{\max}} f(\xi)\mathrm{d}\xi}, & \sigma_{\min} \le \sigma \le \sigma_{\max}, \\ 0, & \sigma_{\max} < \sigma, \end{cases} \tag{3}$$

$$S_{\mathrm{c}} = S\alpha_{\mathrm{c}}, \tag{4}$$

$$S_{\mathrm{I}} = S\alpha_{\mathrm{I}} = S(1 - \alpha_{\mathrm{c}}), \tag{5}$$

where σ denotes the maximum of tensile stress in history, $\sigma_{\min}$ denotes the minimum of tensile strength of all microplanes, $\sigma_{\max}$ denotes the maximum of tensile strength of all microplanes, ξ is an integral variable and $f(\xi)$ denotes a probability density function.

Assuming that the bearing strength σ_{t} of all microplanes obeys a uniform distribution between $[\sigma_{\min}, \sigma_{\max}]$ (as shown in Fig. 3), and the probability density function $f(\sigma)$ is written as

$$f(\sigma) = \frac{1}{\sigma_{\max} - \sigma_{\min}}. \tag{6}$$

Based on Eqs. (2) and (3), the crack ratio α_{c} and intact ratio α_{I} can be written as

$$\alpha_{\mathrm{c}} = \begin{cases} 0, & \sigma < \sigma_{\min}, \\ \dfrac{\sigma - \sigma_{\min}}{\sigma_{\max} - \sigma_{\min}}, & \sigma_{\min} \le \sigma \le \sigma_{\max}, \\ 1, & \sigma_{\max} < \sigma, \end{cases} \tag{7}$$

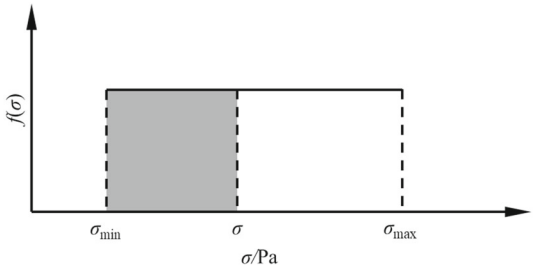

Fig. 3 Probability density function of bearing strength

$$\alpha_{\mathrm{I}}=\begin{cases}1, & \sigma<\sigma_{\min},\\ \frac{\sigma_{\max}-\sigma}{\sigma_{\max}-\sigma_{\min}}, & \sigma_{\min}\le\sigma\le\sigma_{\max},\\ 0, & \sigma_{\max}<\sigma.\end{cases}\tag{8}$$

Because broken microplanes no longer bear load, the external force F_{L} can be written as

$$F_{\mathrm{L}}=\sigma S_{\mathrm{I}}=\sigma S,\ \alpha_{\mathrm{I}}=\begin{cases}\sigma S, & \sigma<\sigma_{\min},\\ \frac{-\sigma^2+\sigma\sigma_{\max}}{\sigma_{\max}-\sigma_{\min}}S, & \sigma_{\min}\le\sigma\le\sigma_{\max},\\ 0, & \sigma_{\max}<\sigma.\end{cases}\tag{9}$$

According to Eq. (9), it can be concluded that the maximum of external force F_{L} appears when σ is in the stress range $[\sigma_{\min}, \sigma_{\max}]$. Since the expression of F_{L} in the stress range $[\sigma_{\min}, \sigma_{\max}]$ is a unary quadratic equation, it can be concluded that the maximum of F_{L} (i.e., the macro-bearing capacity F_{ma}) appears when σ is equal to $\sigma_{\max}/2$ based on the characteristic of unary quadratic equation. In addition, the expression of F_{ma} is different when the correspondence between $\sigma_{\min}$ and $\sigma_{\max}/2$ is different.

The expression of macro-bearing capacity F_{ma} is written as

$$F_{\mathrm{ma}}=\begin{cases}\frac{S}{\sigma_{\max}-\sigma_{\min}}(-\sigma_{\min}^2+\sigma_{\max}\sigma_{\min}), & \text{if } \sigma_{\min}\ge\frac{\sigma_{\max}}{2},\\ \frac{S}{\sigma_{\max}-\sigma_{\min}}\frac{\sigma_{\max}^2}{4}, & \text{if } \sigma_{\min}<\frac{\sigma_{\max}}{2}.\end{cases}\tag{10}$$

Since the bearing strength σ_{t} of all microplanes obeys a uniform distribution between $[\sigma_{\min}, \sigma_{\max}]$, it can be concluded that the average value of bearing strength is $(\sigma_{\min} + \sigma_{\max})/2$. Therefore, the sum of bearing capacity of all microplanes is written as

$$F_{\mathrm{sum}}=\iint_S \sigma_{\mathrm{t}}\mathrm{d}s=\frac{\sigma_{\min}+\sigma_{\max}}{2}S.\tag{11}$$

Then, a brief analysis is conducted to determine the correspondence between F_{ma} and F_{sum}, and the expression is written as

$$\text{If}\quad \sigma_{\min}\ge\frac{\sigma_{\max}}{2},$$

$$(\sigma_{\max}-\sigma_{\min})^2>0,$$

$$\sigma_{\max}^2-\sigma_{\min}^2>-2\sigma_{\min}^2+2\sigma_{\max}\sigma_{\min},$$

$$\frac{\sigma_{\max}+\sigma_{\min}}{2}S>\frac{-\sigma_{\min}^2+\sigma_{\max}\sigma_{\min}}{\sigma_{\max}-\sigma_{\min}}S.\tag{12}$$

$$\text{If}\quad \sigma_{\min}<\frac{\sigma_{\max}}{2},$$

$$\sigma_{\max}^2>2\sigma_{\min}^2,$$

$$2\sigma_{\max}^2-2\sigma_{\min}^2>\sigma_{\max}^2,$$

$$\frac{\sigma_{\max}+\sigma_{\min}}{2}S>\frac{S}{\sigma_{\max}-\sigma_{\min}}\frac{\sigma_{\max}^2}{4}.\tag{13}$$

According to Eqs. (12) and (13), it can be concluded that F_{sum} is always larger than F_{ma} whether $\sigma_{\min}$ is larger than $(\sigma_{\min} + \sigma_{\max})/2$ or $\sigma_{\min}$ is smaller than $(\sigma_{\min} + \sigma_{\max})/2$.

The above analysis shows that once the damage of entire plane is progressive, the macro-bearing capacity F_{ma} will be always smaller than the sum F_{sum} of bearing capacity of all microplanes. Therefore, it can be concluded that the correspondence between F_{ma} and F_{sum} in the case of progressive damage is different from the correspondence between F_{ma} and F_{sum} in the case of simultaneous damage.

2.2 Damage-aggravation effect

In current mechanical analysis, it is determined that the macro-bearing capacity F_{ma} is equal to the sum F_{sum} of bearing capacity of all microplanes, that is, a model will be destroyed only when the external force is equal to F_{sum}. However, the theoretical analysis in "Difference of the macro-bearing capacity" section shows that the correspondence that $F_{\mathrm{ma}} = F_{\mathrm{sum}}$ is valid only in the case of simultaneous damage. Once the damage of all microplanes does not occur simultaneously, F_{ma} will be smaller than F_{sum}, and it indicates that progressive damage will lead to a decrease in the macro-bearing capacity F_{ma}. The progressive damage in "Difference of the macro-bearing capacity" section is caused by the non-uniformity of bearing strength. However, in the field of geotechnical engineering, local defect, non-uniformity of geometry, non-uniformity of external load and non-uniformity of mechanical parameters are all important factors that cause the appearance of progressive damage.

With the increase of local defect, non-uniformity of geometry and non-uniformity of mechanical parameters, the progressive characteristic of damage becomes more obvious. Compared with simultaneous damage, the number and area of crack planes in the progressive damage process are larger, which indicates that the degree of damage is more serious. This phenomenon that more damage occurs in the progressive damage process is defined as "damage-aggravation effect" of progressive damage, and it can be observed that

"damage-aggravation effect" emphasizes the degree of damage in progressive damage is more serious than that in simultaneous damage. From a mechanical point of view, the key factor in the appearance of "damage-aggravation effect" is stress redistribution. Once a part of the structure is damaged, the stress will be redistributed and other parts will be damaged. Based on the "damage-aggravation effect" caused by stress redistribution, it can be concluded that compared with simultaneous damage, the degree of damage to structure in the progressive damage process increases, and the stability of structure decreases. Therefore, F_{ma} is smaller than F_{sum} in the case of progressive damage. In addition, with the increase of non-uniformity of mechanical parameters, the "damage-aggravation effect" becomes more obvious, and it causes F_{ma} to decrease continuously.

Quantifying the "damage-aggravation effect" is of significance for accurately evaluating the macro-bearing capacity F_{ma} of a structure. Because the mechanical parameters and some breaking criterions are involved in the progressive damage process, it is difficult to accurately describe "damage-aggravation effect" solely by the geometrical parameters (e.g., the area and number of crack planes). Therefore, it is proposed to establish a dimensionless indicator to quantify "damage-aggravation effect" based on mechanical parameters and geometrical parameters.

2.3 Progressive damage ratio K_t

Progressive damage has time scale and spatial scale. For a crack plane, its generation and propagation last for a period of time. For several crack planes, their generation and propagation do not occur simultaneously. Therefore, progressive damage has time scale. In addition, because the crack planes are randomly distributed inside the model, progressive damage has spatial scale. Considering the characteristic of progressive damage and the effect of external force, the dimensionless indicator should have four characteristics: (1) It can reflect the "damage-aggravation effect" of progressive damage; (2) It can represent all damage generated from the initial moment of loading to the current moment; (3) It can represent the changing trend of damage at the current moment; (4) It can reflect the influence of different external force on progressive damage. Based on the above characteristics, progressive damage ratio K_t is proposed.

The schematic diagram of crack propagation is plotted in Fig. 4. The black dotted line indicates the crack boundary at time t, and the black solid line indicates the crack boundary at time $t+\Delta t$. When the external force is applied on model, some crack planes appear inside the model, and the tip of a crack plane is located at point O at time t. With the increase of loading time, these crack planes gradually propagate, and the tip of this crack plane is located at point A at time $t+\Delta t$. Because the crack opening displacement is infinitely small,

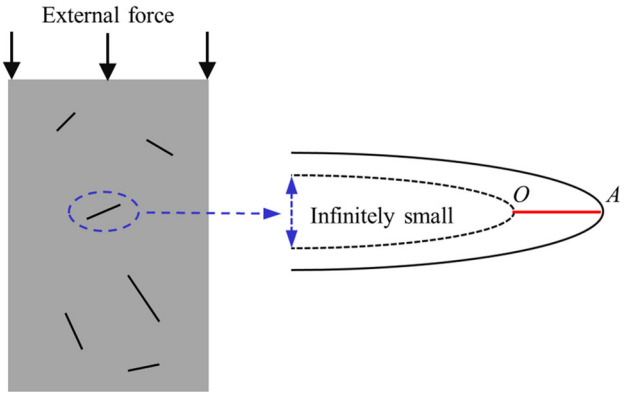

Fig. 4 Process of crack propagation

the distance between point O and point A can be regarded as the crack propagation length, and the crack propagation length is indicated by solid red line in Fig. 4.

When the external force is constant, the progressive damage ratio K_t is written as

$$S_{\mathrm{c}}^{t}=\sum_{N_{\mathrm{c}}^{t}} v_i^t B_i,$$

$$F_t^{'}=\iint_{S_{\mathrm{c}}^{t}} \sigma \mathrm{d}s,$$

$$K_t=\frac{F_{\mathrm{c}}^{t}}{F_{\mathrm{b}}}=\frac{\int_0^t F_t^{'}\mathrm{d}t}{F_{\mathrm{b}}}, \tag{14}$$

where S_{c}^{t} (unit: $\mathrm{m}^2\ \mathrm{s}^{-1}$) denotes the area of new crack planes at time t, N_{c}^{t} denotes the number of crack planes at time t, v_i^t (unit: $\mathrm{m\ s}^{-1}$) denotes the crack propagation rate of i-th crack plane at time t, B_i (unit: m) denotes the characteristic width of i-th crack plane, σ (unit: Pa) denotes the bearing strength of crack planes, $F_t^{'}$ (unit: $\mathrm{N\ s}^{-1}$) denotes the change rate of the sum of bearing capacity of all crack planes at time t, F_{c}^{t} denotes the sum of bearing capacity of all crack planes up to time t, F_{b} (unit: N) denotes the external force applied on model. These symbols are scalars, and they only denote the value of vectors and tensors.

In Eq. (14), the area of new crack planes at time t is calculated firstly. As shown in Fig. 4, the crack propagation rate v_i^t of i-th crack plane is equal to $|OA|/\Delta t$ when Δt is infinitely equal to 0. In addition, because new crack planes are two-dimensional planes and v_i^t only represents the crack propagation length per unit time, the extended area of i-th crack plane is obtained by multiplying v_i^t by the characteristic width B_i of i-th crack plane. After the area S_{c}^{t} of new crack planes at time t is calculated, the change rate $F_t^{'}$ of the sum of bearing capacity of all crack planes at time t is obtained by integrating the bearing strength σ with the area S_{c}^{t} of new crack planes. Subsequently, the sum F_{c}^{t} of bearing capacity of all crack planes is calculated by integrating the

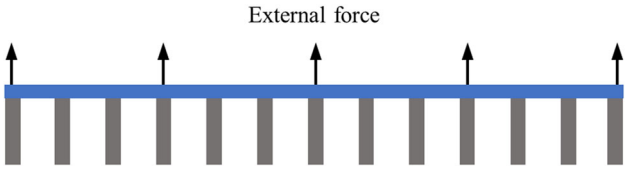

Fig. 5 Rod model

change rate $F_t^{'}$ with time t. Finally, progressive damage ratio K_t is calculated by dividing F_c^t by the external force F_b.

It can be observed that progressive damage ratio K_t is the ratio of F_c^t, the sum of bearing capacity of all crack planes, to external force F_b. In the formula, the denominator denotes external force applied on model, and it can be concentrated force, surface force and body force. The numerator denotes the sum of bearing capacity of all crack planes up to time t. Since it gradually increases with the increase of loading time, it is written as an integral form of time to reflect the time scale of progressive damage. The integrand function $F_t^{'}$ denotes the change rate of the sum of bearing capacity of all crack planes at time t, and it is obtained by integrating bearing strength σ with the area of new crack planes, reflecting the spatial scale of progressive damage. Therefore, it can be concluded that the expression of K_t can reflect the time scale and spatial scale of progressive damage. With the increase of loading time, new crack planes continuously appear, and K_t gradually increase.

3 Parameter study

The rod model (as shown in Fig. 5) is established to study the relationship between some influencing factors and K_t. There are several vertical rods underneath, and each rod can bear tensile force, compressive force and shear force. There is a horizontal rod above the vertical rods, and it is used to transfer the external force F_L to all vertical rods. N_r denotes the number of vertical rods in the model. F_i denotes the bearing capacity of i-th vertical rod, and F_{sum} denotes the sum of bearing capacity of all vertical rods. Once the load of a vertical rod is larger than the bearing capacity, this vertical rod will be destroyed, and its load will be transferred to other vertical rods. There are two eigenvalue (i.e., F_{min} and F_{ma}) of F_L: no rod breaks if $F_L < F_{min}$, only some rods break if $F_{min} \le F_L < F_{ma}$, and all rods break if $F_{ma} \le F_L$. It can be concluded that F_{ma} is the macro-bearing capacity of rod model (i.e., the maximum of external force F_L that the rod model can bear).

The factors affecting the final value of K_t include the bearing capacity F_i, the order of arrangement O_r, the number N_s of affected rods and the distributed ratio α. F_i denotes the maximum of load that i-th rod can bear. Since the load will be redistributed after the failure of rods, the bearing capacity of these rods around the broken rods plays an important role in the mechanical response of rod model. O_r is proposed to characterize the spatial distribution of bearing capacity, and in the rod model, O_r denotes the sequence arrangement of rods with different bearing capacity from left to right. In addition, in order to characterize the spatial region of stress redistribution, N_s is proposed, and it denotes the number of rods whose load will change after the failure of a rod. Besides, since the load of surrounding rods will change once a rod breaks, α is proposed to accurately characterize the change of load of surrounding rods. The distributed ratio α can be regard as an array which includes N_s data, and the added load of i-th rod around the broken rod is equal to the load of broken rod multiplied by α_i.

It is assumed that the elastic modulus of all rods is same and the load will be immediately transferred to surrounding rods after a rod breaks. The correspondence between F_{ma}, the final value of K_t and influencing factors is analyzed.

The research object in Fig. 4 is a continuous model, and some quantities (i.e., $F_t^{'}$ and F_c^t) are expressed in an integral form. However, the research object in Fig. 5 is several discrete rods, and these quantities (i.e., $F_t^{'}$ and F_c^t) cannot expressed in an integral form. Therefore, the calculation of K_t is simplified and the expression is written as

$$K_t = \frac{F_c^t}{F_b} = \frac{\sum_{N_c^t} F_i}{F_b}, \tag{15}$$

where F_c^t denotes the sum of bearing capacity of all broken rods up to time t, N_c^t denotes the number of broken rods up to time t, F_i denotes the bearing capacity of i-th rod, and F_b denotes the external force.

It can be concluded that the main difference between Eqs. (14) and (15) is the expression of F_c^t. The expression of F_c^t in Eq. (14) is an integral form, and the expression of F_c^t in Eq. (15) is an accumulation form, but the meaning that they express is same.

3.1 Theoretical analysis

When all vertical rods are intact, the external force is evenly distributed. Once a rod is broken, its load will be borne by several surrounding rods, and the non-uniform distribution of external force appears. In this case, F_i, O_r, N_s and α have influences on the final value of K_t. Currently, there is no suitable index to quantify the order of arrangement O_r. Therefore, the order of arrangement O_r of vertical rods in this section is fixed, and it is determined that the bearing capacity F_i of vertical rods gradually increases from left to right in the rod model. It is assumed that the number N_r of vertical rods in the rod model is equal to 200. Under the premise, the corre-

spondence between F_{ma}, the final value of K_t and influencing factors is analyzed.

3.1.1 Bearing capacity F_i

The weibull distribution, normal distribution and uniform distribution are used to randomize the bearing capacity F_i under the premise that $F_{\mathrm{sum}} = 200$ kN. It is assumed that the number N_{s} of affected rods is equal to 1. Therefore, when a vertical rod breaks, the load that it bears will be transferred to N_{s} rods on the left side and right side. If there is no rod on one side, the load will be transferred to N_{s} rods on the other side. The changing trends of F_{max} and the final value of K_t under different distribution forms of F_i are explored and plotted in Fig. 6. The dimensionless quantity λ_{F} is proposed to characterize the dispersion degree of bearing capacity F_i, and the expression is written as

$$\lambda_{\mathrm{F}} = \frac{F_{\mathrm{st}}}{\overline{F}}, \tag{16}$$

where F_{st} denotes the standard deviation of bearing capacity F_i, $\overline{F}$ denotes the average value of bearing capacity F_i.

Under the premise that the sum F_{sum} of bearing capacity remains unchanged, it can be observed that with the increase of λ_{F}, the macro-bearing capacity F_{ma} decreases, and the final value of K_t increases. It indicates that the "damage-aggravation effect" gradually enhances. However, the changing trends of F_{ma} and K_t under different distribution are different, and when λ_{F} under different distribution forms of F_i is same, the value of F_{ma} and K_t is different. When the dimensionless quantity λ_{F} is 0, it means that the bearing capacity F_i of each rod is equal to 1 kN, and it can be observed that the macro-bearing capacity F_{ma} is equal to the sum F_{sum} of bearing capacity of all vertical rods. Therefore, it can be concluded that there is no "damage-aggravation effect" when the bearing capacity of all rods is same, and the progressive damage ratio $K_t = 1$.

Taking the uniform distribution as an example, the bearing capacity F_i is regarded as an arithmetic progression to simplify the theoretical analysis process, and it can be concluded that the dimensionless quantity λ_{F} is linear with the minimum of bearing capacity F_i under the premise that F_{sum} remains unchanged. The value of bearing capacity F_i from smallest to largest is $F_1, F_2, \ldots, F_{\mathrm{Nr}}$, and Δ denotes the common difference of arithmetic progression. Based on the value of bearing capacity F_i, it can be concluded that F_1 is always larger than Δ in this question.

The breaking criterion of i-th rod is written as

$$F_1 + (i-1)\Delta \le \frac{F_{\mathrm{L}}}{N_{\mathrm{r}}} + (i-1)\frac{F_{\mathrm{L}}}{N_{\mathrm{r}}}, \quad 1 \le i \le N_{\mathrm{r}}, \tag{17}$$

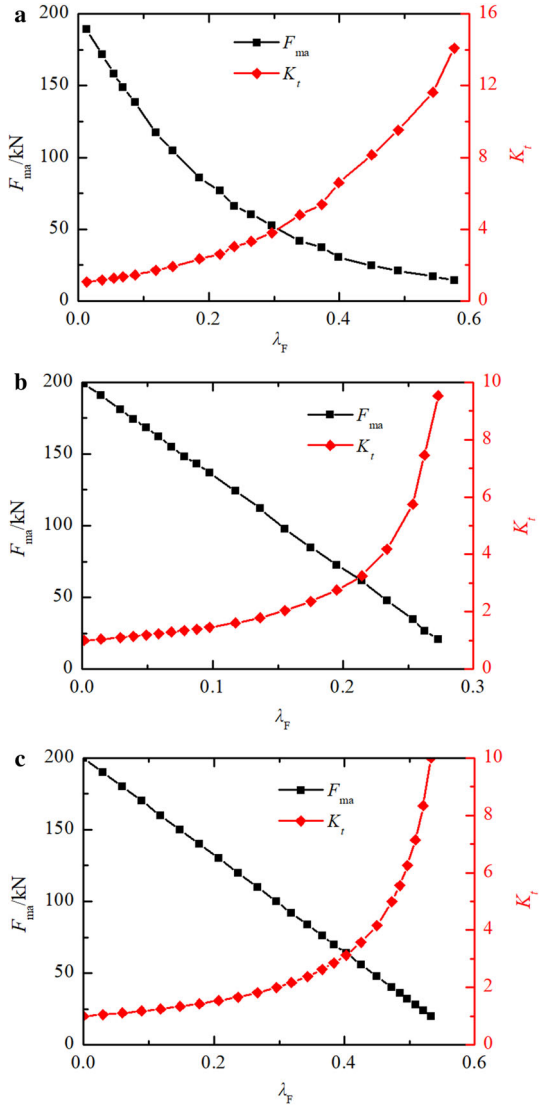

Fig. 6 Changing curves of K_t and F_{ma} under different distribution forms of F_i ($\overline{F} = 1$ kN). **a** Weibull distribution, **b** normal distribution, and **c** uniform distribution

where F_1 denotes the minimum of bearing capacity of rods, F_{L} denotes the external force, and N_{r} denotes the number of vertical rods.

Because F_1 is larger than Δ, it can be concluded that as long as the breaking criterion of the first rod is satisfied, the breaking criterion of all rods will be satisfied, and the macro-bearing capacity F_{ma} is equal to $F_1 N_{\mathrm{r}}$. With the increase of λ_{F}, F_1 decreases linearly, and the macro-bearing capacity F_{ma} also decreases linearly. Based on the definition of K_t, it can be observed that K_t increases inversely with the linear decrease of F_{ma}.

With $\lambda' = F_1/\overline{F}$ as the horizontal axis, the fitting curves of K_t and F_{ma} are plotted in Fig. 7. The fitting formula of F_{ma} is $F_{\mathrm{ma}} = 200\lambda'$, and the fitting formula of K_t is $K_t =$

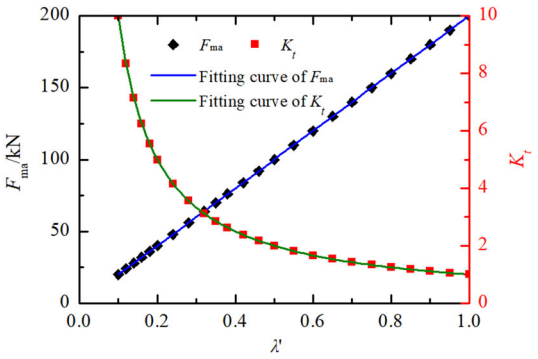

Fig. 7 Fitting curves of K_t and F_{ma}

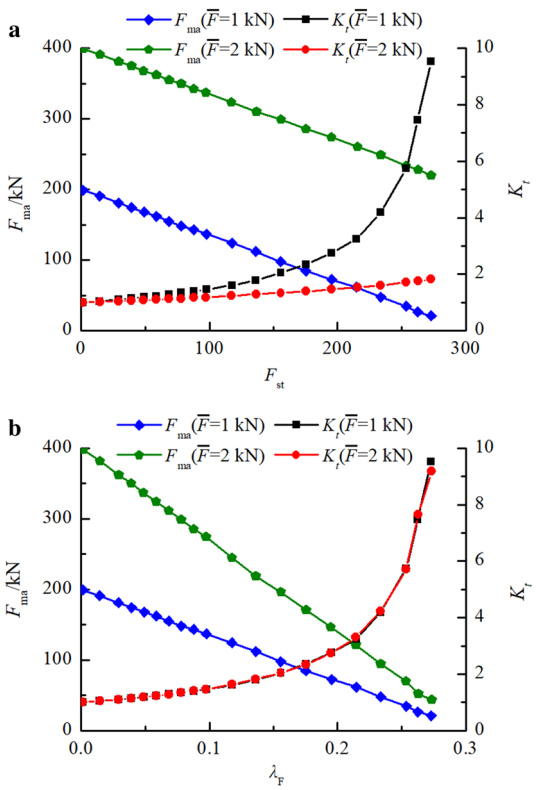

Fig. 8 Changing curves of F_{ma} and K_t under normal distribution **a** with the same value of F_{st} and **b** with the same value of λ_F

$1/\lambda'$. It can be observed that the result is consistent with the conclusion of theoretical analysis.

In Fig. 6, under the premise that the sum F_{sum} of bearing capacity remains unchanged, the changing trends of F_{ma} and K_t are studied. A further research is conducted to investigate the influences of average value $\overline{F}$ on the changing trends of F_{ma} and K_t.

It is assumed that the bearing capacity F_i obeys normal distribution. In first case, under the premise that the standard deviation F_{st} of bearing capacity is same and the average value $\overline{F}$ of bearing capacity is different, the changing trends of F_{ma} and K_t are investigated and plotted in Fig. 8a. In second case, it is assumed that the standard deviation F_{st} and average value $\overline{F}$ are different, but λ_F is same, the changing trends of F_{ma} and K_t are investigated and plotted in Fig. 8b.

Based on Fig. 8a, it can be observed that the average value $\overline{F}$ has a great influence on the changing trends of F_{ma} and K_t. When the standard deviation F_{st} of bearing capacity is same, with the increase of average value $\overline{F}$, the macro-bearing capacity F_{ma} increases and the progressive damage ratio K_t decreases. It indicates that the damage-aggravation effect gradually weakens with the increase of $\overline{F}$ when the standard deviation F_{st} is same. Therefore, it can be concluded that F_{st} is not enough to characterize the dispersion degree of bearing capacity when studying the changing laws of progressive damage ratio K_t. Based on Fig. 8(b), it is observed that although the average value $\overline{F}$ and the standard deviation F_{st} are different, the changing trend of progressive damage ratio K_t is same with the increase of λ_F. and the value of K_t is same when λ_F is same. Therefore, it is concluded that λ_F is more applicable to characterize the dispersion degree of bearing capacity when studying the changing laws of progressive damage ratio K_t.

In Fig. 6, it is observed that with the increase of λ_F, the changing trends of F_{ma} are different. When the bearing capacity F_i of rods obeys uniform distribution or normal distribution, F_{ma} decreases linearly with the increase of λ_F. When the bearing capacity F_i of rods obeys weibull distribution, F_{ma} decreases nonlinearly with the increase of λ_F. A brief analysis is conducted to investigate the reasons for different changing trends.

At the initial moment of loading, the external load is evenly transferred to N_r rods, and the load on each rod is F_L/N_r. Because the bearing capacity F_i of rods gradually increases from left to right in the rod model, the failure of rods starts from the left side firstly. Once a rod breaks, the load on this rod will be immediately transferred to the adjacent rod on the right. The failure criterions of i-th rod and $(i+1)$-th rod are written as

$$\begin{aligned} F_i &\le \frac{F_L}{N_r} i, \\ F_{i+1} &\le \frac{F_L}{N_r}(i+1). \end{aligned} \tag{18}$$

It can be concluded that if $F_{i+1} - F_i$ is always smaller than F_L/N_r, as long as the failure criterion of first rod is satisfied, the failure criterions of all rods will be satisfied. Based on the bearing capacity of rods, it can be observed that F_1 is always larger than $F_{i+1} - F_i$ whether F_i is randomized by uniform distribution, normal distribution or weibull distribution. Therefore, the external load F_L that satisfies the failure criterion of the first road is the macro-bearing capacity F_{ma} of

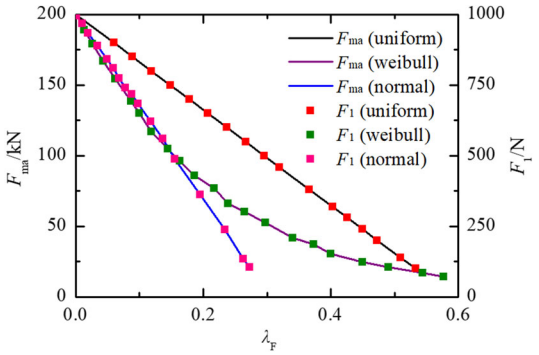

Fig. 9 Changing trends of F_{ma} and F_1

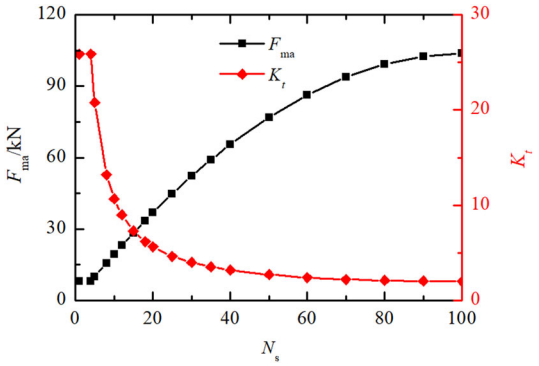

Fig. 10 Changing curves of K_t and F_{ma}

entire model. The changing trends of F_{ma} and F_1 are plotted in Fig. 9.

According to Fig. 9, it can be observed that the changing trends of F_1 and F_{ma} are consistent under the same distribution function, and F_{ma} is equal to $F_1 N_r$. Because of the algorithm characteristics of different distribution functions, the changing trends of F_1 are different with the linear increase of λ_F. Therefore, the changing trends of F_{ma} are different when the bearing capacity F_i is randomized by different functions.

3.1.2 Number N_s of affected rods

It is assumed that the bearing capacity F_i of rods obeys uniform distribution, the minimum of bearing capacity F_i is $F_r^{min} = 40$ N, the maximum of bearing capacity F_i is $F_r^{max} = 2030$ N, and the sum of bearing capacity of all rods is $F_{sum} = 207$ kN. The effect of N_s on the macro-bearing capacity F_{ma} and progressive damage ratio K_t is studied by changing the value of N_s. When a vertical rod breaks, the load that it bears will be evenly transferred to N_s rods on the left and right side. If there is no rod on one side, the load will be transferred to N_s rods on the other side. The changing trends of the final value of K_t and the macro-bearing capacity F_{ma} when N_s changes are investigated and plotted in Fig. 10.

According to Fig. 10, it can be observed that F_{ma} and K_t remain unchanged when N_s is smaller than a certain value. Therefore, it can be concluded that the change of N_s does not affect "damage-aggravation effect" when N_s is in a certain value range. Once N_s is larger than a certain value, with the increase of N_s, F_{ma} increases nonlinearly, and the final value of K_t decreases nonlinearly. It indicates that "damage-aggravation effect" gradually decreases with the increase of N_s.

When the bearing capacity F_i of vertical rods obeys uniform distribution, the bearing capacity F_i is regarded as an arithmetic progression to simplify the theoretical analysis process. The value of bearing capacity F_i from smallest to largest is $F_1, F_2, \ldots, F_{Nr}$, and Δ denotes the common difference of arithmetic progression. An eigenvalue N_o (the largest integer not larger than F_1/Δ) is defined, and it can be divided into two cases of $N_s \le N_o$ and $N_s > N_o$ according to the correspondence between N_s and N_o.

In the case of $N_s \le N_o$, the breaking criterion of i-th rod is written as

$$\begin{aligned} F_1 + (i-1)\Delta &\le \frac{F_L}{N_r} + (i-1)\frac{F_L}{N_r}\frac{1}{N_s}, \qquad 1 \le i \le (N_r - N_s + 1), \\ F_1 + (i-1)\Delta &\le \frac{F_L}{N_r} + (i-1)\frac{F_L}{N_r}\frac{1}{N_r + 1 - i}, \quad (N_r - N_s + 1) < i \le N_r. \end{aligned} \tag{19}$$

It can be concluded that as long as the breaking criterion of the first rod is satisfied, the breaking criterion of all rods will be satisfied. Therefore, the macro-bearing capacity of entire rod model is $F_{ma} = F_1 N_r = 8000$ N.

In the case of $N_s > N_o$, the breaking criterion of i-th rod is written as

$$\begin{aligned} F_1 + (i-1)\Delta &\le \frac{F_L}{N_r} + (i-1)\frac{F_L}{N_r}\frac{1}{N_s}, \qquad 1 \le i \le (N_r - N_s + 1), \\ F_1 + (i-1)\Delta &\le \frac{F_L}{N_r} + (i-1)\frac{F_L}{N_r}\frac{1}{N_r + 1 - i}, \quad (N_r - N_s + 1) < i \le N_r. \end{aligned} \tag{20}$$

Based on the correspondence between N_s and N_o, it can be concluded that as long as the breaking criterion of $i = N_r - N_s + 1$ rod is satisfied, the breaking criterion of all rods will be satisfied. The macro-bearing capacity of entire rod model is written as

$$F_{ma} = [F_1 + (N_r - N_s)\Delta]N_s. \tag{21}$$

Based on Eq. (21), it can be observed that F_{ma} is the quadratic function of N_s.

With N_s as the horizontal axis, the fitting curves of F_{ma} and K_t are plotted in Fig. 11. The fitting formula of F_{ma} is written as

$$F_{ma} = -0.01N_s^2 + 2.04N_s. \tag{22}$$

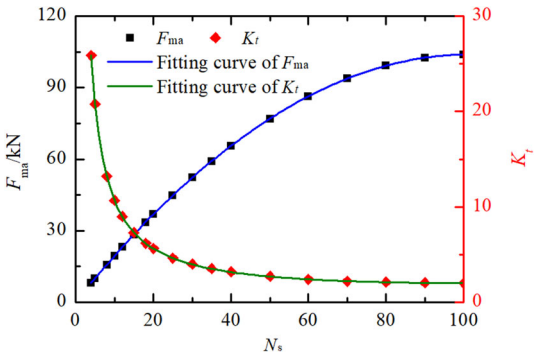

Fig. 11 Fitting curves of K_t and F_{ma}

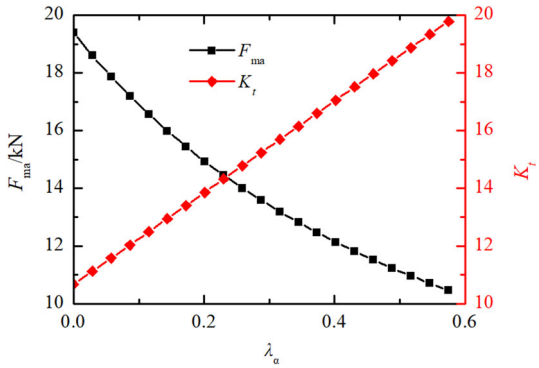

Fig. 12 Changing curves of K_t and F_{ma}

The fitting formula of K_t is written as

$$K_t = 207/(-0.01N_s^2 + 2.04N_s). \tag{23}$$

It can be observed that the result is consistent with the conclusion of theoretical analysis.

3.1.3 Distributed ratio α

It is assumed that the bearing capacity F_i of rods obeys uniform distribution, the minimum of bearing capacity is $F_r^{min} = 40$ N, the maximum of bearing capacity is $F_r^{max} = 2030$ N, and the sum of bearing capacity of all rods is $F_{sum} = 207$ kN, Besides, the number of affected rods is $N_s = 10$. The distributed ratio α is an array which includes N_s data, and it is assumed that the data obeys uniform distribution. The added load of i-th rod around a broken rod is equal to the load of broken rod multiplied by α_i. Because the sum of added load of surrounding rods is equal to the load of broken rod, it can be concluded that the sum of α_i is 1, and it is written as:

$$\alpha_1+\alpha_2+\ldots+\alpha_{N_s}= 1. \tag{24}$$

In order to simplify the theoretical analysis, it is determined that the distributed ratio α remains unchanged for all rods. However, when the number N_d of intact rods on one side is less than N_s, α_i increases to $\alpha_i N_s/N_d$ so that the sum of added load of surrounding rods is always equal to the load of broken rod.

The dimensionless quantity λ_α is proposed to characterize the dispersion degree of distributed ratio α, and it is written as

$$\lambda_\alpha = \frac{\alpha_{st}}{\overline{\alpha}}, \tag{25}$$

where α_{st} denotes the standard deviation of distributed ratio α, and $\overline{\alpha}$ denotes the average value of distributed ratio α.

The changing trends of macro-bearing capacity F_{ma} and the final value of K_t are plotted in Fig. 12. Under the premise that F_{sum} and N_s remain unchanged, it can be observed that with the increase of λ_α, F_{ma} decreases nonlinearly and K_t increases linearly.

When the bearing capacity F_i of vertical rods obeys uniform distribution, the bearing capacity F_i is regarded as an arithmetic progression to simplify the theoretical analysis process. The value of bearing capacity F_i from smallest to largest is $F_1, F_2, \ldots, F_{Nr}$, Δ denotes the common difference of arithmetic progression, and the maximum of distributed ratio is α_{max}.

Under the premise that the number of affected rods is $N_s = 10$, it can be observed that there are exactly 10 rods in the rod model when 1–190 rods have been broken from left to right. Therefore, the added load of 191-th rod is equal to the load of 190-th rod multiplied by α_{max}. However, when the 191-th rod also breaks, there are only 9 rods in the rod model. It can be concluded that the distributed ratio α should be increased to ensure that the load of broken rods can be fully borne by intact rods. From the above analysis, it can be concluded that the distributed ratio of 1–191 rods is α_{max}, and the distributed ratio of 192–200 rods increases to 10 $\alpha_{max}/(201 - i)$. Therefore, $i = 191$ and $i = 192$ are chosen as the dividing point.

The breaking criterion of i-th rod is written as

$$\begin{cases} F_1 + (i-1)\Delta \le \dfrac{F_L}{N_r} + \alpha_{max}(i-1)\dfrac{F_L}{N_r}, & i \le 191, \\ F_1 + (i-1)\Delta \le \dfrac{F_L}{N_r} + \alpha_{max}(i-1)\dfrac{F_L}{N_r}\dfrac{10}{201-i}, & 192 \le i \le 200. \end{cases} \tag{26}$$

It can be concluded that as long as the breaking criterion of $i = 191$ rod is satisfied, the breaking criterion of all rods will be satisfied. The macro-bearing capacity of entire rod model is written as

$$F_{ma} = (F_1 + 190\Delta)N_r/(1 + 190\alpha_{max}). \tag{27}$$

Based on the expression of progressive damage ratio K_t, it can be concluded that with the increase of α_{max}, F_{ma} decreases nonlinearly and K_t increases linearly.

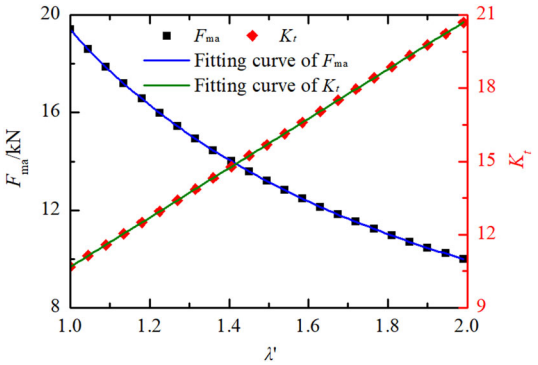

Fig. 13 Fitting curves of K_t and F_{ma}

With $\lambda' = \alpha_{max}/\overline{\alpha}$ as the horizontal axis, the fitting curves of F_{ma} and the final value of K_t are plotted in Fig. 13. The fitting formula of F_{ma} is written as

$$F_{ma} = 388/(1 + 19\lambda'). \tag{28}$$

The fitting formula of K_t is written as

$$K_t = 10.14\lambda' + 0.53. \tag{29}$$

It can be concluded that the result is consistent with the conclusion of theoretical analysis.

3.2 Numerical simulation

The correspondence between F_{max}, the final value of K_t and some influencing factors has been investigated based on theoretical analysis. In this section, the continuum-discontinuum element method (CDEM) [52, 53] is used to study the correspondence between F_{max}, the final value of K_t and the non-uniformity of bearing capacity F_i.

3.2.1 Basic concept

The CDEM is a dynamic explicit algorithm, and the governing equation of CDEM is established through Lagrange energy system. The numerical model of CDEM is composed of interface and block. A block includes one or more elements, and it is used to represent the continuous features of material. The interface is located at the common boundary between two blocks, and it is used to represent the discontinuous features. The interface is constituted of the real interface and the virtual interface. The real discontinuous features of material are represented by the real interface. The virtual interface has two main purposes: one is to connect two blocks and transfer mechanical information, and the other is to provide a potential space for crack generation and propagation. In order to achieve the accurate calculation of contact force and failure state, a semi-spring and semi-edge combined contact model is introduced into CDEM.

The Mohr–Coulomb fracture criterion (Eq. (30)) and maximum tensile stress criterion (Eq. (31)) are selected as the failure criterion of interface.

$$\begin{cases} \text{If } F_s \geq F_n \tan\varphi + c_p s, \\ F_s = F_n \tan\varphi + c_p s, \\ \text{next step } c_p = 0,\ \sigma_{pt} = 0. \end{cases} \tag{30}$$

$$\begin{cases} \text{If } -F_n \geq \sigma_{pt} s, \\ F_n = F_s = 0, \\ \text{next step } c_p = 0,\ \sigma_{pt} = 0, \end{cases} \tag{31}$$

where σ_{pt} denotes the spring tensile strength, c_p denotes the spring cohesive strength, φ denotes the spring friction angle, and s denotes the spring contact area.

3.2.2 Simplified form of K_t

Because CDEM adopts explicit solution method, the interface will immediately crack if it meets the failure criterion. Therefore, it is difficult to quantify the crack propagation rate v_i^t of new crack planes in Eq. (14). In addition, for each independent crack plane, it is not as infinitely small as the microplane in theoretical analysis. Therefore, it is necessary to simplify the computing formula Eq. (14) to achieve the accurate computation of K_t in CDEM.

In Eq. (14), firstly, the area of new crack planes at time t is obtained, and then F_t' is obtained by integrating the bearing strength with area. Secondly, F_c^t is obtained by integrating F_t' with time. This calculation can accurately reflect the time scale and spatial scale of progressive damage. However, because of the algorithm limitations of CDEM, Eq. (14) cannot directly used in CDEM to obtain the value of K_t, Therefore, the calculation process of F_c^t is simplified, and the new expression is written as

$$K_t = \frac{F_c^t}{F_b} = \frac{\sum \sigma_i s_i}{\frac{N_c^t}{F_b}} \tag{32}$$

where N_c^t denotes the number of crack planes that have appeared up to time t, σ_i denotes the bearing strength of i-th crack plane, s_i denotes the area of i-th crack plane, F_b denotes the external force, and F_c^t denotes the sum of bearing capacity of all crack planes up to time t.

It can be observed that the continuous crack planes are regarded as a set of independent crack planes. Therefore, the expressions of F_c^t in integral form become the expressions of F_c^t in accumulative form.

Based on Eq. (32), some code is developed in CDEM to calculate F_c^t and F_b. Firstly, the number of crack planes that have appeared up to time t is counted, and the area and bearing

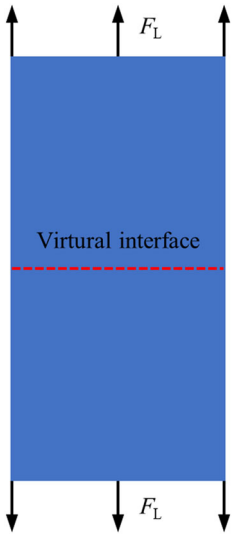

Fig. 14 Numerical model

strength of each crack plane are also obtained. Therefore, the sum of bearing capacity of all crack planes up to time t is calculated. Then the value of external force F_b is obtained based on the type of external force (i.e., concentrated force, surface force and body force). Finally, progressive damage ratio K_t is calculated according to Eq. (32).

3.2.3 Numerical result

In order to study the correspondence between F_{ma}, the final value of K_t and the non-uniformity of bearing capacity F_i by CDEM, a numerical model (0.05 m × 0.1 m) is established and shown in Fig. 14, and it includes 2500 elements. The density is $\rho = 2400$ kg/m^3, and the elastic modulus is $E = 2$ GPa. The upper and lower boundaries are subjected to surface force, and there are virtual interfaces in the middle of model. The elements adopt linear elastic constitutive law and the interfaces adopt brittle fracture constitutive law. Based on the algorithm characteristics of CDME, it can be concluded that some springs are arranged at the virtual interfaces. The springs are used to simulate the vertical rods in the rod model, and the elements are used to transfer external force. Therefore, it can be concluded that this numerical model can accurately reflect the structural and mechanical characteristics of rod model. The tensile strength of springs obeys uniform distribution. Under the premise that the sum of bearing capacity of all springs is $F_{sum} = 100$ kN, the upper and lower limit of distribution range are continuously adjusted to study the changing trends of F_{ma} and the final value of K_t.

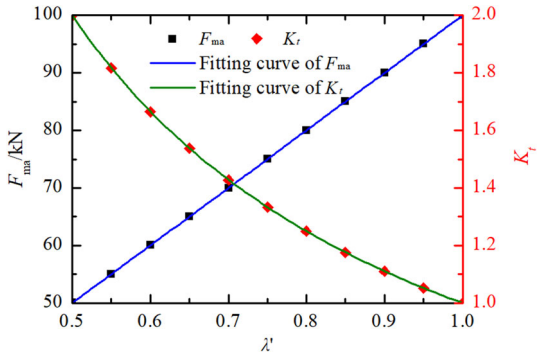

Fig. 15 Changing curves of K_t and F_{ma}

Based on numerical result, the changing trends of F_{ma} and K_t are plotted in Fig. 15. λ' is a newly proposed dimensionless indicator, and the expression is written as

$$\lambda' = \frac{F_r^{min}}{\overline{F}}, \tag{33}$$

where F_r^{min} denotes the minimum of bearing capacity F_i, and $\overline{F}$ denotes the average value of bearing capacity F_i.

According to Fig. 15, it can be observed that with the increase of λ', F_{ma} increases linearly, and the error between F_{ma} and F_{sum} gradually decreases. When the bearing capacity F_i of all springs is same, F_{ma} is equal to F_{sum}. It can be concluded that the non-uniformity of bearing capacity F_i is a key factor affecting the macro-bearing capacity F_{ma}. In addition, Fig. 15 illustrates that with the increase of λ', the final value of K_t decreases inversely. It indicates that "damage-aggravation effect" gradually weakens. When the bearing capacity of all springs is same, the crack of all springs occurs simultaneously, and there is no "damage-aggravation effect" (i.e., $K_t = 1$).

The fitting formula of F_{ma} is written as $F_{ma} = 100\,\lambda'$, and the fitting formula of K_t is written as $K_t = 1/\lambda'$.

The numerical result shows that the "damage-aggravation effect" does exist and the non-uniformity of bearing capacity is a key factor that causes the occurrence of progressive damage. Once the bearing capacity F_i is distributed, the progressive damage process will occur, and it leads to the "damage-aggravation effect". The correspondence between these values obtained by numerical simulation is consistent with that obtained by theoretical analysis in "Theoretical analysis" section. When the bearing capacity F_i obeys uniform distribution, with the increase of non-uniformity of F_i, F_{ma} decreases linearly and the final value of K_t increases inversely.

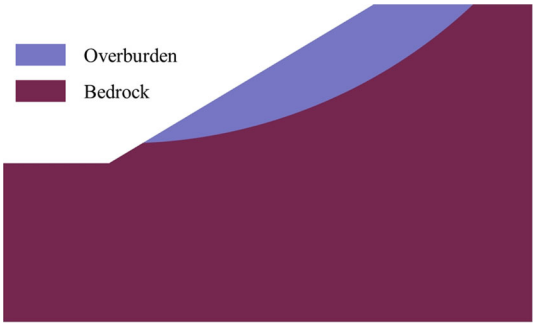

Fig. 16 2D slope model

4 Discussion

This study serves as a proof-of-concept that "damage-aggravation effect" caused by stress redistribution in progressive damage process does exist. Since the rod model cannot reflect the complex stress redistribution process, a 2D slope model is established to investigate the effect of progressive damage on the stability of entire slope and study whether the "damage-aggravation effect" really exist. The numerical model is plotted in Fig. 16, and the mechanical parameters are shown in Table 1. In order to characterize the non-uniformity of mechanical parameters, it is assumed that the friction angle of overburden obeys normal distribution, with expectation $u = 20$ and standard deviation $\sigma = 5$.

The failure process of entire slope is shown in Fig. 17, and the black lines indicate crack planes. It can be observed that there are a few crack planes at the interface between overburden and bedrock at the initial moment. Because of the effect of stress redistribution, more and more crack planes appear, and ultimately the entire interface breaks.

The numerical results indicate that the entire slope is unstable. However, based on limit equilibrium method (Fellenius method), since the anti-sliding force of entire slope is 5.83×10^6 N and the sliding force of entire slope is 4.94×10^6 N, it can be concluded that this slope is stable and the safety factor is 1.18. It can be observed that the result of limit equilibrium method is inconsistent with the result of numerical simulation. Since the failure of entire interface between overburden and bedrock is progressive, it can be concluded the anti-sliding force of entire slope is not equal to the sum of anti-sliding force of all sliding slices, and the anti-sliding force of entire slope should be corrected based on progressive damage ratio K_t. It is determined that the progressive damage ratio $K_t = 1.21$ based on the numerical result. Therefore, the anti-sliding force of entire slope is equal to the sum of anti-sliding force of all sliding slices divided by 1.21, and it is 4.82×10^6 N. According to the corrected anti-sliding force of entire slope, it can be concluded that the slope is unstable and the safety factor is 0.98.

Based on the numerical simulation of slope, it can be observed that once the damage of complex engineering structure is progressive, "damage-aggravation effect" will appear because of the stress redistribution, and it leads to the macro-bearing capacity of entire structure is not equal to the sum of bearing capacity of all parts. Therefore, it can be concluded that there are some deficiencies in limit equilibrium method and it needs to be corrected. In addition, since the progressive damage really exists in many fields, the influence of stress redistribution on the macro-bearing capacity of entire structure should be considered.

The core purpose of introducing progressive damage ratio K_t is to evaluate the macro-bearing capacity F_{ma} of entire structure more accurately. Usually, it is determined that the macro-bearing capacity F_{ma} is equal to the sum F_{sum} of bearing capacity of all parts. However, the correspondence between F_{ma} and F_{sum} changes once the damage is progressive. Therefore, progressive damage ratio K_t is proposed, and the macro-bearing capacity F_{ma} is corrected based on K_t in order to characterize the influence of "damage-aggravation effect" and evaluate the stability of entire structure more accurately.

Take the limit equilibrium method as an example. Firstly, the sum F_{sum} of anti-sliding force of all sliding slices is obtained, and it is not equal to the anti-sliding force of entire slope because of the existence of progressive damage. Then, a more accurate anti-sliding force of entire slope is obtained by dividing the sum of anti-sliding force of all sliding slices by K_t. Therefore, it can be concluded that K_t quantify the influence of "damage-aggravation effect" on the macro-bearing capacity F_{ma}, and F_{ma} is equal to F_{sum} divided by K_t. When the damage occurs simultaneously, F_{ma} is equal to F_{sum} because of $K_t = 1$. In order to determine F_{ma} more accurately, the progressive damage ratio K_t should be determined accurately. However, due to the complexity of stress redistribution, more work needs to be done to obtain the changing law of progressive damage ratio K_t.

Table 1 Mechanical parameters

Material	Density/(kg m^{-3})	Elastic modulus/MPa	Poisson ratio	Cohesion strength/kPa	Friction angle/(°)
Overburden	2400	250	0.25	20	20
Bedrock	2750	500	0.2	40	40

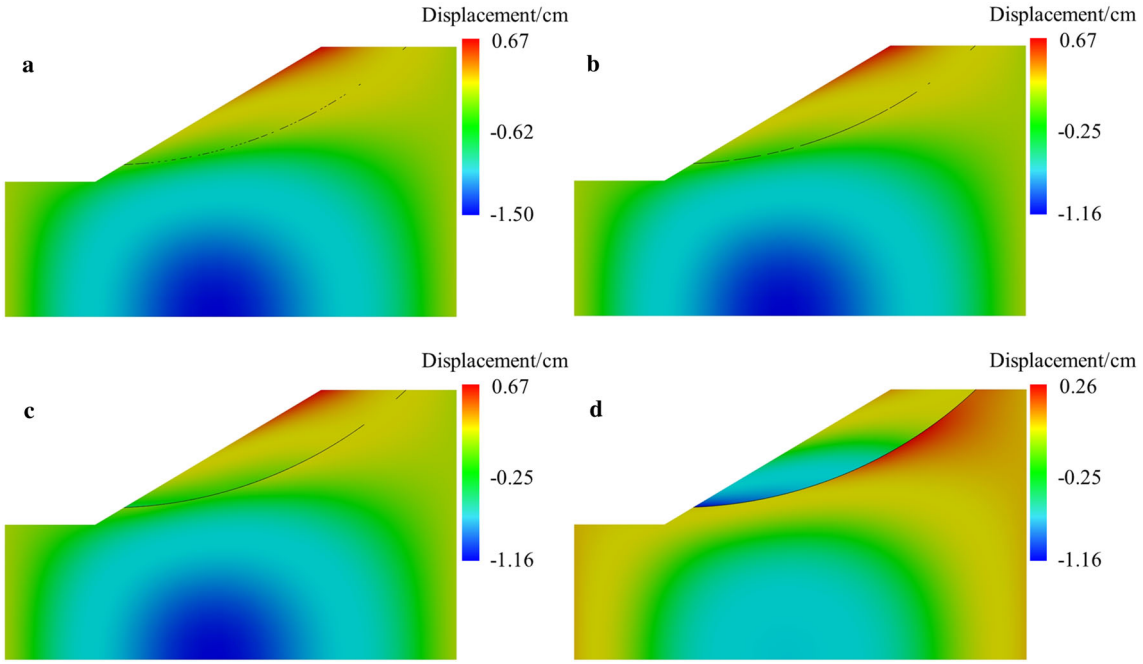

Fig. 17 Failure process of entire slope. **a** Time step = 2475, **b** time step = 2490, **c** time step = 2570, and **d** time step = 3200

5 Conclusions

Aiming at the progressive damage process in many fields, a quantitative study on the correspondence between the sum F_{sum} of bearing capacity of all crack planes and the macro-bearing capacity F_{ma} is conducted. Firstly, based on the theoretical analysis of a 2D plane inside the RVE, it is concluded that the correspondence between F_{sum} and F_{ma} is different in the case of simultaneous damage and progressive damage, and "damage-aggravation effect" is proposed. Then progressive damage ratio K_t is proposed to quantify "damage-aggravation effect". Finally, based on the rod model, the correspondence between some influencing factors and progressive damage ratio K_t is obtained through theoretical analysis, and the correspondence between the non-uniformity of bearing capacity and K_t obtained by theoretical analysis is verified based on numerical simulation.

The following conclusions are obtained.

1. Both theoretical analysis and numerical simulation show that "damage-aggravation effect" does exist when the failure of model is progressive. Unlike $F_{\text{sum}} = F_{\text{ma}}$ in the case of simultaneous damage, F_{sum} is larger than F_{ma} in the case of progressive damage. It indicates that the macro-bearing capacity of model is reduced in the case of progressive damage.
2. Based on the rod model, the theoretical analysis shows that the bearing capacity F_i of rods, the number N_{s} of affected rods and the distributed ratio α have an effect on the macro-bearing capacity F_{ma}. If the bearing capacity F_i obeys uniform distribution, with the linear increase of maximum of F_i, F_{ma} increases linearly and K_t decreases inversely. When N_{s} is in a certain value range, with the linear increase of N_{s}, F_{ma} increases quadratically. As the maximum of distributed ratio α increases linearly, F_{ma} decreases inversely, and K_t increases linearly.
3. The numerical simulation result is consistent with the theoretical result in terms of the correspondence between the macro-bearing capacity F_{ma}, the progressive damage ratio K_t and the non-uniformity of bearing capacity F_i. Besides, the validity of K_t in quantifying "damage-aggravation effect" is verified.

In further research, the changing laws of macro-bearing capacity F_{ma} and progressive damage ratio K_t in complicated working conditions will be studied in detail, and the modified form of limit equilibrium method will be established based on progressive damage ratio K_t. In addition, the expression of K_t under time-dependent load will be established and the correspondence between K_t and influencing factors under time-dependent load will be studied.

Acknowledgements The authors would like to acknowledge the financial support of the National Key Research and Development Project of China, the Ministry of Science and Technology of China (Grant 2018YFC1505504).

References

1. Liu, G., Zhang, L., Guo, L., et al.: Multi-scale progressive failure simulation of 3D woven composites under uniaxial tension. Compos. Struct. **208**, 233–243 (2019)
2. Lin, Y., Huang, Y., Huang, T., et al.: Characterization of progressive damage behaviour and failure mechanisms of carbon fibre reinforced aluminium laminates under three-point bending. Thin. Wall. Struct. **135**, 494–506 (2019)
3. Zhao, L., Yang, W., Cao, T., et al.: A progressive failure analysis of all-C/SiC composite multi-bolt joints. Compos. Struct. **202**, 1059–1068 (2018)
4. Hu, X.F., Haris, A., Ridha, M., et al.: Progressive failure of bolted single-lap joints of woven fibre-reinforced composites. Compos. Struct. **189**, 443–454 (2018)
5. Guerrero, J.M., Mayugo, J.A., Costa, J., et al.: A 3D progressive failure model for predicting pseudo-ductility in hybrid unidirectional composite materials under fibre tensile loading. Compos. Part. A. Appl. Sci. Manuf. **107**, 579–591 (2018)
6. Zhou, S., Yang, C., Tian, K., et al.: Progressive failure modelling of double-lap of composite bolted joints based on Puck's criterion. Eng. Fract. Mech. **206**, 233–249 (2019)
7. Zuo, Y., Montesano, J., Singh, C.V.: Assessing progressive failure in long wind turbine blades under quasi-static and cyclic loads. Renew. Energ. **119**, 754–766 (2018)
8. Banat, D., Mania, R.J.: Progressive failure analysis of thin-walled fibre metal laminate columns subjected to axial compression. Thin. Wall. Struct. **122**, 52–63 (2018)
9. Rivera, J.A., Aguilar, E., Cárdenas, D., et al.: Progressive failure analysis for thin-walled composite beams under fatigue loads. Compos. Struct. **154**, 79–91 (2016)
10. Bai, Y., Zhang, X.Z.: Progressive failure analysis of open-hole composite hoops under radial loading. Compos. B Eng. **97**, 336–343 (2016)
11. Stephen, D., Lam, D., Forth, J., et al.: An evaluation of modelling approaches and column removal time on progressive collapse of building. J. Constr. Steel. Res. **153**, 243–253 (2019)
12. Rahnavard, R., Fard, F.F.Z., Hosseini, A., et al.: Nonlinear analysis on progressive collapse of tall steel composite buildings. Case. Stud. Constr. Mater. **8**, 359–379 (2018)
13. He, J., Pan, F., Cai, C.S., et al.: Progressive failure analysis of low-rise timber buildings under extreme wind events using a DAD approach. J. Wind. Eng. Ind. Aerodyn. **182**, 101–114 (2018)
14. Elsanadedy, H.M., Almusallam, T.H., Alharbi, Y.R., et al.: Progressive collapse potential of a typical steel building due to blast attacks. J. Constr. Steel. Res. **101**, 143–157 (2014)
15. Eberhardt, E., Stead, D., Coggan, J.S.: Numerical analysis of initiation and progressive failure in natural rock slopes—the 1991 randa rockslide. Int. J. Rock. Mech. Min. Sci. **41**, 69–87 (2004)
16. Jiang, X.G., Wörman, A., Chen, P.S., et al.: Mechanism of the progressive failure of non-cohesive natural dam slopes. Geomorphology **363**, 1–11 (2020)
17. Nishimura, T., Fukuda, T., Tsujino, K.: Distinct element analysis for progressive failure in rock slope. Soils. Found. **50**, 505–513 (2010)
18. Tang, S.B., Huang, R.Q., Tang, C.A., et al.: The failure processes analysis of rock slope using numerical modelling techniques. Eng. Fail. Anal. **79**, 999–1016 (2017)
19. Wang, B., Vardon, P.J., Hicks, M.A.: Investigation of retrogressive and progressive slope failure mechanisms using the material point method. Comput. Geotech. **78**, 88–98 (2016)
20. Ye, G.L., Zhang, F., Yashima, A., et al.: Numerical analyses on progressive failure of slope due to heavy rain with 2D and 3D FEM. Soils. Found. **45**, 1–15 (2005)
21. Kong, L., Ostadhassan, M., Hou, X., et al.: Microstructure characteristics and fractal analysis of 3D-printed sandstone using micro-CT and SEM-EDS. J. Pet. Sci. Eng. **175**, 1039–1048 (2019)
22. Li, H.M., Li, H.G., Wang, K., et al.: Effect of rock composition microstructure and pore characteristics on its rock mechanics properties. Int. J. Min. Sci. Technol. **28**, 303–308 (2018)
23. Rahman, T., Lebedev, M., Zhang, Y., et al.: Influence of rock microstructure on its electrical properties: an analysis using X-ray microcomputed tomography. Energy. Procedia. **114**, 5023–5031 (2017)
24. Radlinski, A.P., Ioannidis, M.A., Hinde, A.L., et al.: Angstrom-to-millimeter characterization of sedimentary rock microstructure. J. Colloid. Interface. Sci. **274**, 607–612 (2004)
25. Doroshkevich, A.G., Veksler, I.V., Klemd, R., et al.: Trace-element composition of minerals and rocks in the belaya zima carbonatite complex (Russia): implications for the mechanisms of magma evolution and carbonatite formation. Lithos **284**, 91–108 (2017)
26. Sun, H., Belhaj, H., Tao, G., et al.: Rock properties evaluation for carbonate reservoir characterization with multi-scale digital rock images. J. Pet. Sci. Eng. **175**, 654–664 (2019)
27. Sun, H., Vega, S., Tao, G.: Analysis of heterogeneity and permeability anisotropy in carbonate rock samples using digital rock physics. J. Pet. Sci. Eng. **156**, 419–429 (2017)
28. He, T.M., Zhao, Q., Ha, J., et al.: Understanding progressive rock failure and associated seismicity using ultrasonic tomography and numerical simulation. Tunn. Undergr. Space. Technol. **81**, 26–34 (2018)
29. Guo, S., Qi, S.: Numerical study on progressive failure of hard rock samples with an unfilled undulate joint. Eng. Geol. **193**, 173–182 (2015)
30. Fukuyama, E., Tsuchida, K., Kawakata, H., et al.: Spatiotemporal complexity of 2-D rupture nucleation process observed by direct monitoring during large-scale biaxial rock friction experiments. Tectonophysics **733**, 182–192 (2018)
31. Rodríguez, P., Celestino, T.B.: Application of acoustic emission monitoring and signal analysis to the qualitative and quantitative characterization of the fracturing process in rocks. Eng. Fract. Mech. **210**, 54–69 (2018)
32. Dai, F., Xu, Y., Zhao, T., et al.: Loading-rate-dependent progressive fracturing of cracked chevron-notched Brazilian disc specimens in split Hopkinson pressure bar tests. Int. J. Rock. Mech. Min. Sci. **88**, 49–60 (2016)
33. Liu, S., Li, X., Li, Z., et al.: Energy distribution and fractal characterization of acoustic emission (AE) during coal deformation and fracturing. Measurement **136**, 122–131 (2019)
34. Wei, M.D., Dai, F., Xu, N.W., et al.: Experimental and numerical study on the fracture process zone and fracture toughness determination for ISRM-suggested semi-circular bend rock specimen. Eng. Fract. Mech. **154**, 43–56 (2016)
35. Liu, B., Ma, Y.J., Zhang, G., et al.: Acoustic emission investigation of hydraulic and mechanical characteristics of muddy sandstone experienced one freeze-thaw cycle. Cold. Reg. Sci. Technol. **151**, 335–344 (2018)
36. Shen, J., Liu, B.G., Cheng, Y., et al.: Experimental research on mechanical properties of diabase under uniaxial and conventional triaxial compression. Sci. Technol. Eng. **20**, 5297–5304 (2020)
37. Xie, H.P., Liu, J.F., Ju, Y., et al.: Fractal property of spatial distribution of acoustic emissions during the failure process of bedded rock salt. Int. J. Rock. Mech. Min. Sci. **48**, 1344–1351 (2011)
38. Yang, J., Mu, Z.L., Yang, S.Q.: Experimental study of acoustic emission multi-parameter information characterizing rock crack development. Eng. Fract. Mech. **232**, 1–15 (2020)
39. Wang, C.L., Hou, X.L., Li, H.T., et al.: Experimental investigation on dynamic evolution characteristics of micro-cracks for sandstone samples under uniaxial compression. Chinese J. Geotech. Eng. **41**, 2120–2125 (2019)

40. Deng, J., Gu, D.S.: On a statistical damage constitutive model for rock materials. Comput. Geosci. **37**, 122–128 (2011)
41. Gao, W., Chen, X., Hu, C.J., et al.: New damage evolution model of rock material. Appl. Math. Model. **86**, 207–224 (2020)
42. Lin, H., Xie, S.J., Yong, R., et al.: An empirical statistical constitutive relationship for rock joint shearing considering scale effect. C R Phys. **347**, 561–575 (2019)
43. Liu, X.S., Tan, Y.L., Ning, J.G., et al.: Mechanical properties and damage constitutive model of coal in coal-rock combined body. Int. J. Rock. Mech. Min. Sci. **110**, 140–150 (2018)
44. Nguyen, C.T., Nguyen, G.D., Das, A., et al.: Constitutive modelling of progressive localised failure in porous sandstones under shearing at high confining pressures. Int. J. Rock Mech. Min. Sci. **93**, 179–195 (2017)
45. Xie, S.J., Lin, H., Chen, Y.F., et al.: A damage constitutive model for shear behavior of joints based on determination of the yield point. Int. J. Rock. Mech. Min. Sci. **128**, 104269 (2020)
46. Heidarpour, F., Farahani, M., Ghabezi, P.: Experimental investigation of the effects of adhesive defects on the single lap joint strength. Int. J. Adhes. Adhes. **80**, 128–132 (2018)
47. Kamiya, S., Kita, T., Izumi, H.: Defect accumulation and strength reduction in single crystalline silicon induced by cyclic compressive stress. Sens. Actuator. A. Phys. **208**, 30–36 (2014)
48. Liu, G., Cai, M., Huang, M.: Mechanical properties of brittle rock governed by micro-geometric heterogeneity. Comput. Geotech. **104**, 358–372 (2018)
49. Liakas, S., O'Sullivan, C., Saroglou, C.: Influence of heterogeneity on rock strength and stiffness using discrete element method and parallel bond model. J. Rock. Mech. Geotech. Eng. **9**, 575–584 (2017)
50. Manouchehrian, A., Cai, M.: Influence of material heterogeneity on failure intensity in unstable rock failure. Comput. Geotech. **71**, 237–246 (2016)
51. Li, S., Zhou, D.: Progressive failure constitutive model of fracture plane in geomaterial based on strain strength distribution. Int. J. Solids. Struct. **50**, 570–577 (2013)
52. Ju, Y., Liu, P., Chen, J., et al.: CDEM-based analysis of the 3D initiation and propagation of hydrofracturing cracks in heterogeneous glutenites. J. Nat. Gas. Sci. Eng. **35**, 614–623 (2016)
53. Feng, C., Li, S., Liu, X., et al.: A semi-spring and semi-edge combined contact model in CDEM and its application to analysis of Jiweishan landslide. J. Rock. Mech. Geotech. Eng. **6**, 26–35 (2014)